Aerosol direct radiative effect over clouds from synergy of OMI and MODIS reflectance

Martin de Graaf[1], L. Gijsbert Tilstra[1], and Piet Stammes[1]

[1]Satellite Observations Department, Royal Netherlands Meteorological Institute (KNMI), De Bilt, The Netherlands

Correspondence: M. de Graaf, Royal Netherlands Meteorological Institute, R&D Satellite Observations Department, Utrechtseweg 297, De Bilt, The Netherlands, martin.de.graaf@knmi.nl

Abstract. The retrieval of geophysical parameters is increasingly dependent on synergistic use of satellite instruments. More sophisticated parameters can be retrieved and the accuracy of retrievals can be increased when more information is combined. In this paper, a synergistic application of OMI/Aura and MODIS/Aqua Level 1B reflectances is described, enabling the retrieval of the aerosol direct radiative effect (DRE) over clouds using the differential aerosol absorption (DAA) technique. This technique

5   was first developed for reflectances from SCIAMACHY/Envisat, which had the unique capability of measuring contiguous radiances from the ultraviolet (UV) at 240 nm to 1750 nm in the shortwave-infrared (SWIR), at a moderate spectral resolution of 0.2–1.5 nm. However, the spatial resolution and global coverage of SCIAMACHY was limited, and Envisat stopped delivering data in 2012. In order to continue the DRE data retrieval, reflectances from OMI and MODIS, flying in formation, were combined from the UV to the SWIR. This resulted in reflectances at a limited but sufficient spectral resolution, available at

10   the OMI pixel grid, which have a much higher spatial resolution and coverage than SCIAMACHY. The combined reflectance spectra allow the retrieval of cloud microphysical parameters in the SWIR, and the subsequent retrieval of aerosol DRE over cloud scenes using the DAA technique. The new aerosol DRE over clouds dataset from OMI/MODIS is compared to the SCIAMACHY dataset for the period 2006–2009, showing a very high correlation. The average aerosol DRE over clouds in August 2006 was 31.5 Wm^{-2} with a standard deviation of 16 Wm^{-2}. The maximum daily averaged DRE from OMI/MODIS

15   in August 2006 was 75.6±13 Wm^{-2}. Over the Atlantic Ocean, the OMI/MODIS DRE dataset is related to AOT measurements over Ascension Island in 2016, showing the transport of smoke all the way from its source region in Africa over the Atlantic to Ascension and beyond.

1   Introduction

20   The radiative effect of aerosols is one of the least certain components in global climate models (Yu et al., 2006; Forster et al., 2007). This is mainly due to the aerosol influences on clouds. Aerosols can influence e.g. cloud formation, cloud albedo and cloud life time, through their role as cloud condensation nuclei, which are called the indirect effects of aerosols (e.g.

Haywood and Boucher, 2000; Lohmann and Feichter, 2005). But even the aerosol direct radiative effect (DRE), the component of aerosol radiative forcing that neglects all influences on clouds, is still poorly constrained, due to the heterogeneous distribution of aerosol sources and sinks and the influence of clouds on global observations of aerosols. In particular, the characterisation of aerosol properties in cloudy scenes has proved challenging. Locally, the aerosol DRE can be very large and dominate the radiative forcing. The understanding of aerosol effects and the influence of aerosols on clouds would be greatly

5   advanced with daily monitoring of aerosol DRE from passive instruments with global coverage.

The aerosol DRE can be retrieved over cloud scenes using shortwave reflectance measurements, such as measured by the spaceborne spectrometer Scanning Imaging Absorption Spectrometer for Atmospheric Chartography (SCIAMACHY). By determining cloud optical thickness and droplet effective radius in the SWIR, as opposed to in the visible where absorption due to aerosols can bias the cloud retrievals (Haywood et al., 2004), the aerosol effect can be determined by comparing the true

10   cloud-aerosol scene reflectance with a modelled cloud-only scene reflectance spectrum (de Graaf et al., 2012). The spectral difference between the scene with and without aerosols is quantified by the spectral difference, which is attributed to aerosol absorption, hence the name differential aerosol absorption (DAA).

While satellite instruments have become increasingly sophisticated, measuring at higher spatial and spectral resolution, and retaining global coverage in one day for most polar orbiting satellites, there is a demand for synergistic use of instruments.

15   Space agencies have facilitated the combined use of instruments, by building instruments with complementary functionality and flying them in formation. The best example is the Afternoon constellation (A-Train), currently flying six satellites within minutes of each other, allowing near-simultaneous observation of a wide variety of parameters.

In this paper, DAA is applied to combined observations from the Ozone Monitoring Instrument (OMI) on-board the Aura satellite and from the Moderate Resolution Imaging Spectroradiometer (MODIS) on-board the Aqua satellite, both flying

20   in the A-Train. Additionally, the A-Train provides opportunities for verification and validation of the measurements. Lidar measurements from the Cloud-Aerosol Lidar with Orthogonal Polarization (CALIOP) lidar onboard the CALIPSO satellite in the A-Train are used here to complement the aerosol DRE measurements with accurate cloud and aerosol characterisation. Polarimeter measurements from the Polarization and Directionality of the Earth's Reflectance (POLDER) data can be used to simultaneously derive aerosol optical thickness (AOT) and cloud optical thickness (COT) in a scene, from which the aerosol

25   DRE over clouds can also be derived (Peers et al., 2015). In an accompanying paper, POLDER aerosol DRE over clouds is compared with the OMI/MODIS derived DRE (de Graaf et al., 2019). Additionally, in the current paper, a comparison is provided with the original retrieval of aerosol DRE over clouds using SCIAMACHY data.

This paper is organised as follows: Section 2 describes the retrieval of the aerosol DRE from hyperspectral reflectance measurements in the shortwave spectrum domain using DAA. Section 3 describes the synergy of OMI and MODIS reflectances,

30   to create a hyperspectral reflectance spectrum with sufficient spectral resolution to apply DAA. Section 4 shows the aerosol DRE over clouds in the south-east Atlantic Ocean from OMI/MODIS, compared to the aerosol DRE over clouds, derived from SCIAMACHY hyperspectral measurements from 2006 to 2009. During these years both instruments produced accurate measurements and the SCIAMACHY data from these years have been analysed extensively in previous publications. In section 5,

additional aerosol DRE data for the years 2016 and 2017 are presented, in support of aerosol-cloud interaction studies in the

35 Atlantic basin which have been performed in this area during those years.

2 Theory

2.1 Aerosol direct effect

The instantaneous aerosol DRE at the top of the atmosphere (TOA) is defined as the change in net (upwelling minus down-welling) irradiance, due to the introduction of aerosols in the atmosphere. Since the downwelling radiation is simply the

5 incoming solar radiation, and assuming negligible aerosol effects in the longwave radiation spectrum, for a cloud scene the aerosol DRE is

$$\mathrm{DRE}_{\mathrm{aer}} = \mathrm{SW}_{\mathrm{cld}}^{\uparrow} - \mathrm{SW}_{\mathrm{cld+aer}}^{\uparrow}, \tag{1}$$

where $\mathrm{SW}_{\mathrm{cld}}^{\uparrow}$ is the shortwave upwelling irradiance in an aerosol-free cloud scene, and $\mathrm{SW}_{\mathrm{cld+aer}}^{\uparrow}$ is the shortwave upwelling irradiance of the same scene with both clouds and aerosols. Equation 1 is equally valid for cloud free scenes, but since the

10 shortwave reflectance can be very small over dark scenes, the DRE would be the difference of very small numbers, yielding highly uncertain DREs. Therefore, only cloudy scenes are considered. Note however, that this yields only positive aerosol DREs, while aerosol DRE over dark surfaces are generally negative as aerosol scattering dominates.

2.2 Differential Aerosol Absorption technique

The aerosol DRE over clouds is determined from shortwave hyperspectral measurements of passive imagers, using measured

15 reflectances of cloud scenes. The Earth reflectance is defined as the quotient of the upwelling radiance $I(\lambda)$ and the downwelling solar irradiance $E_0(\lambda)$:

$$R = \frac{\pi I(\lambda)}{\mu_0 E_0(\lambda)}, \tag{2}$$

where μ_0 is the cosine of the solar zenith angle θ_0. If absorbing aerosols are present above the clouds, the measured scene reflectance $R(\lambda)_{\mathrm{cld+aer}}$ will deviate from an aerosol-free cloud scene reflectance $R(\lambda)_{\mathrm{cld}}$. The reflectance difference is attributed

20 to radiation absorption by the aerosols above the clouds, and the resulting direct radiative effect of these aerosols is quantified by integrating the reflectance difference over all wavelengths in the shortwave spectrum and all angles:

$$\mathrm{DRE}_{\mathrm{aer}} = \int\limits_{SW} \frac{(R(\lambda)_{\mathrm{cld}} - R(\lambda)_{\mathrm{cld+aer}})\,\mu_0 E_0(\lambda)}{B(\lambda, \mu_0)_{\mathrm{cld}}} \mathrm{d}\lambda + \epsilon, \tag{3}$$

where $R(\lambda)_{\mathrm{cld}}$ is a simulated aerosol-free cloud reflectance, representative for the measured scene with the aerosols removed. $B(\lambda, \mu_0)$ is the anisotropy factor of a scene, which is a measure of the angular distribution of the reflected radiation for a scene

25 and used to determine the radiance from a uni-directional reflectance measurement. This is determined from the modelled
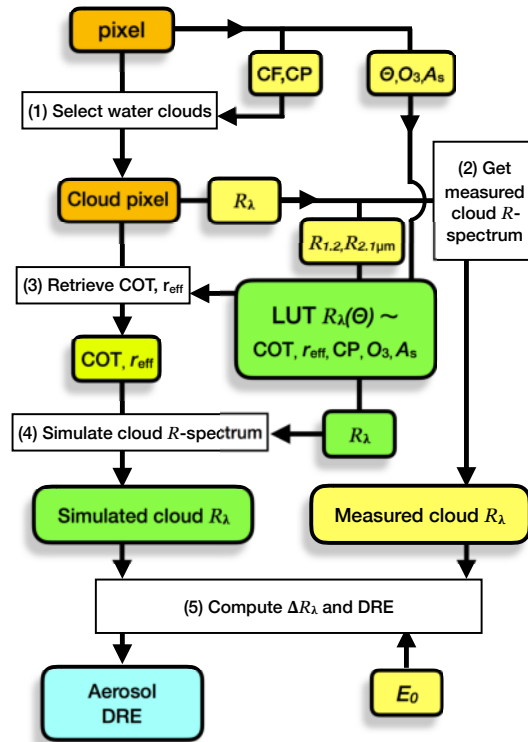
Figure 1. Flow diagram for the Differential Aerosol Absorption technique. Yellow boxes contain pixel products, green boxes contain simulated quantities, the yellow/green box is a retrieval for the cloud pixel and the light blue box is the end product. Θ represents the geometry of the measurements, E_0 is the irradiance spectrum, R_λ is the reflectance (spectrum), CF is cloud fraction, CP is cloud pressure, COT is cloud optical thickness, r_{eff} is cloud droplet effective radius, O_3 is the ozone profile, and A_s is the surface albedo. See text for details.

cloud scene, and assumed to be unchanged by the aerosols over the clouds. ϵ represents all the instrument and retrieval errors of a single measurement. See de Graaf et al. (2012) for a derivation of Equation 3 and a comprehensive treatment of all its components.

The aerosol DRE follows from the integration of the radiance difference between the simulated aerosol-free cloud scene and measured aerosol polluted cloud scene over the solar spectrum. The integration is over the part of the shortwave spectrum where aerosols significantly absorb radiation. In case of combined OMI and MODIS reflectances, the integration limits are from the start of OMI measurements (about 270 nm) to the first of the MODIS channels that are used to invert cloud parameters (1246 nm), where the aerosol absorption is assumed to have become negligible.

An illustration of the DAA technique is given in Figure 1. The first step is the selection of suitable scenes, i.e. the selection of scenes with clouds. To ensure enough clouds only pixels with a cloud fraction (CF) larger than a threshold value (e.g. 0.3) are selected, and to ensure (low level) water clouds, only pixels with a cloud pressure larger than a threshold (e.g. 800 hPa)

10 are selected. Step two is the determination of a measured scene reflectance spectrum. For SCIAMACHY this was trivial, the combination of OMI and MODIS reflectances is treated in section 3.5. Step three is the retrieval of the cloud optical thickness and cloud droplet effective radius, using the SWIR part of the reflectance determined in step two, (e.g. $R_{1.2\mu m}$ and $R_{2.1\mu m}$). The SWIR part of the LUT of reflectances is inverted to retrieve COT and r_{eff} . The fourth step is the simulation of the cloud scene reflectances in the UV, visible and SWIR part of the spectrum. This forward step is simplified using the same LUT as before, which contains reflectances at 18 wavelengths from 295 nm–2130 nm, see table 1. Once the simulated and measured

5 cloud scene reflectances are available, the DRE is computed in step five, using Equation 3 and a measured or reference solar irradiance spectrum $E_0(\lambda)$.

A number of alternatives steps can be identified in this scheme. First, the accuracy of simulating a cloud scene reflectance spectrum can easily be determined by adding an extra selection criterium in step one. The UV aerosol Absorbing Index (UV-AI) has been identified as a very good proxy for the presence of UV-absorbing aerosols in a (cloud) scene (e.g. Wilcox, 2012;

10 Yu and Zhang, 2013; Alfaro-Contreras et al., 2014). By filtering for any cloud scene with a UV-AI larger than 0, scenes with UV-absorbing aerosols above clouds are very effectively filtered. If this criterion is added to step one, the remaining cloud scenes should yield a zero aerosol DRE. The (average) deviation from zero is a good estimate of the uncertainty in simulating the cloud scene reflectance. This is treated in section 4.3 for OMI/MODIS pixels.

Secondly, the determiniation of COT in step three may be replaced by more accurate retrievals. In the current set-up, COT

15 and r_{eff} are retrieved from the measured reflectance spectrum in step three. The SWIR measurements $R_{1.2\mu m}$ and $R_{2.1\mu m}$ are used to avoid biases due to absorption by aerosols, assuming that small particles do not effectively interact with radiation at those wavelengths. This works relatively well, but is also an error source for very thick plumes and larger particles. If unbiased cloud parameters can be obtained from other sources, e.g. from collocated dedicated cloud instruments, the DAA method may be improved, especially for thick aerosol plumes. It may even be extended to cases with desert dust above clouds, which are

20 currently unsuitable, because large mineral particles interact with radiation at SWIR wavelengths.

Table 1. Spectral cloud reflectance LookUp Table nodes

Parameter	Nodes								
wavelength λ [nm]	295	310	320	330	340	380	430	469	555
	610	645	858	867	1051	1240	1246	1640	2130
cloud optical thickness τ_{cld}	2	4	8	12	16	20	24	32	48
droplet size r_{eff} [μm]	3	4	6	8	12	16	20	24	
cloud base height z_{cld} [km]	0	1	4	8	12				
total O_3 column Ω [DU]	267	334	401						
surface albedo A_s	0	0.5	1						
droplet size eff. variance ν_{eff}	0.15								
number of $\theta_0, \theta, \phi - \phi_0$	14	14	19						

3 Measured cloud scene reflectance spectra

3.1 SCIAMACHY

Originally, the DAA technique was applied to reflectance spectra from SCIAMACHY with a cloud fraction larger than 0.3. SCIAMACHY was part of the payload of the Environmental Satellite (Envisat), launched in 2002 into a polar orbit with an equator crossing time of 10:00 LT for the descending node. SCIAMACHY was designed to measure radiation in eight channels from 240–2380 nm at a spectral resolution of 0.2–1.5 nm (Bovensmann et al., 1999). The radiance was observed in

5   two alternating modes, nadir and limb, yielding data blocks called states, approximately 960×480 km^2 in size. A state was divided into 13 swaths. In nadir mode, SCIAMACHY produced unique contiguous reflectance spectra from 240–1750 nm with an optical integration time of 1 s, by co-adding. By interpolating the spectra of pixels with an integration time of 0.25 s, a swath was divided into sixteen pixels of approximately 60×30 km^2. SCIAMACHY stopped delivering data in 2012.

3.2 Instrument synergy using A-Train instruments

10   In order to continue the DRE measurements, a combination of instruments can be used to determine a contiguous reflectance spectrum from the UV to the SWIR. A logical choice were instruments in the Afternoon constellation (A-train), which consists of several satellite platforms flying in constellation in a polar-orbiting, sun-synchronous orbit, crossing the equator in the ascending node during the local afternoon (around 13:30 LT). The purpose is to allow the instruments on-board the platforms observe the same part of the Earth within minutes of each other. The time difference between the instruments within the A-train

15   is controlled by keeping the various satellites within control-boxes, defined as the maximum distances to which the satellites are allowed to drift before correcting maneuvers are executed.

The main focus here is synergistic use of measurements from instruments on-board the Aqua and Aura platforms. Aqua was launched in 2002 and Aura in 2004, following Aqua by about 15 minutes. A major orbital maneuver in 2008 of Aqua decreased the distance between the Aura and Aqua control boxes to about 8 minutes. The scene that is observed by both instruments is

20   variable to a few minutes due to the time difference between Aura and Aqua. Additionally, measurements from the CALIPSO platform in the A-Train were used to illustrate the vertical profile of cloud scenes, but they are not necessary in the derivation of the DRE.

In addition to the combined measurements from Aura and Aqua, a lidar onboard the Cloud-Aerosol Lidar and Infrared Pathfinder Satellite Observation (CALIPSO) was used to illustrate the vertical distribution of the atmosphere. CALIPSO was

25   launched in April 2006 and placed between Aqua and Aura. Therefore, it provides excellent collocation in time with the OMI and MODIS observations. The main payload of CALIPSO is the Cloud-Aerosol Lidar with Orthogonal Polarization (CALIOP) lidar. It provides vertically resolved backscatter profiles of the atmosphere. Here, the Level 1B attenuated backscatter at 532 nm was used, to visualize the vertical distribution of clouds and aerosols of the atmosphere sampled by OMI and MODIS. Since the CALIOP across-track swath is very small, the measurements from CALIOP are representative for the center of the OMI

30   and MODIS swaths only. Note that CALIOP measurements are not needed for the DAA technique.

Table 2. MODIS spectral and spatial specifications of bands 1–7, used in this paper.

Band	Central Wavelength [nm]	Bandwidth [nm]	Spatial resolution [m]
3	469	459 – 479	500
4	555	545 – 565	500
1	645	620 – 670	250
2	858.5	841 – 876	250
5	1240	1230 – 1250	500
6	1640	1628 – 1652	500
7	2130	2105 – 2155	500

3.3 OMI

OMI (Levelt et al., 2006), on-board the Aura satellite, was designed to monitor trace gases in the Earth atmosphere, especially ozone. It was built as the successor to the ESA instruments GOME (Burrows et al., 1999) and SCIAMACHY, and NASA's TOMS instruments (e.g. Fleig et al., 1986; Bhartia et al., 2013). GOME and SCIAMACHY were the first space-borne hyperspectral instruments, measuring the shortwave spectrum from the ultraviolet (UV) to shortwave-infrared (SWIR) wavelength range (up till 800 nm for GOME), from which multiple trace gases, clouds and aerosol parameters can be retrieved simulta-
5   neously. OMI was designed to measure the complete spectrum from the UV to the visible wavelength range (up to 500 nm) with a high spatial resolution and daily global coverage. The optical design of OMI is different from its predecessors, which used scanning mirrors. In OMI, the incoming radiation is projected onto a two dimensional charge-coupled device (CCD). The radiation is split and mapped spectrally in one dimension of the CCD. In the other dimension, the across-track measurements are mapped. The across-track swath width is about 2600 km, resulting in a complete global coverage in one day. The spatial
10   resolution of OMI is typically about $15 \times 23.5\,\mathrm{km}^2$ at nadir to about $42 \times 126\,\mathrm{km}^2$ for far off-nadir (56 degrees) pixels. However, the exact footprint size is complicated, which will be treated explicitly in section 3.5. Since 2008, OMI suffers from progressive degradation, especially in far off-nadir pixels, called the row anomaly.

3.4 MODIS

MODIS is an imaging spectroradiometer and a key instrument on-board the Terra (EOS AM) and Aqua (EOS PM) satellites.
15   MODIS acquires data in 36 spectral bands spanning the visible and infrared. Typical application of MODIS reflectances are measurements of the surface albedo, ocean color and phytoplankton content, trace gases, clouds and aerosols, at a high spatial resolution. In this paper, only the shortwave spectral bands are used, which typically have a spatial resolution of 250–500 m, and a band width of about 20-50 nm. The spatial and spectral specifications of the MODIS bands that are used in this paper are given in Table 2.
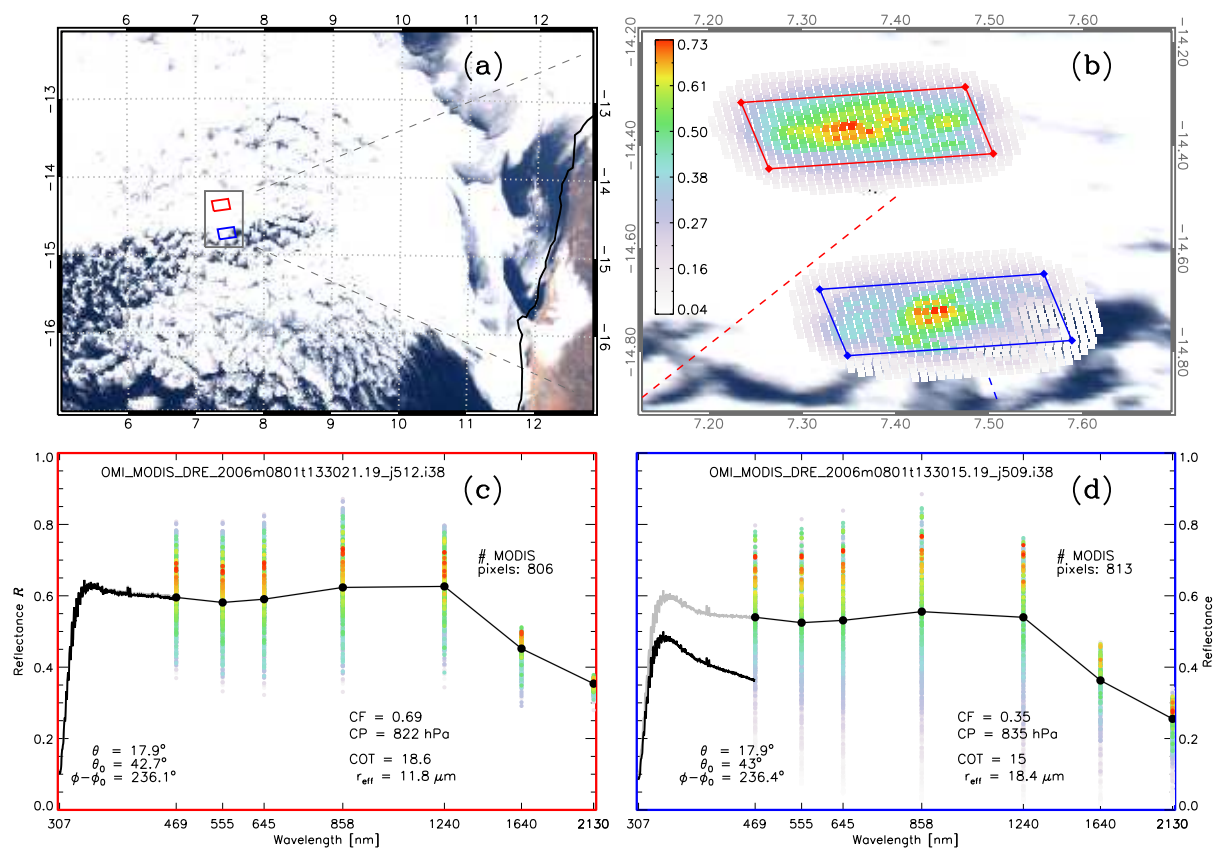
Figure 2. Illustration of the computation of the Aerosol DRE from a combination of one OMI pixels and collocated MODIS pixels. (a) Overview of a stratocumulus cloud deck over the south-east Atlantic Ocean using MODIS RGB, and two selected OMI pixels, in red and blue; (b) Close-up of the two selected OMI pixels, with collocated high resolution MODIS pixels, coloured by their intensity, which is determined by the MODIS reflectance, convolved with the OMI pixel point spread function, which is used to weigh the contribution of the individual MODIS pixels; (c) Shortwave spectrum from the red OMI pixel combined with the average MODIS reflectance (black). The coloured dots indicate the weight of the individual MODIS pixels; (d) Shortwave spectrum of the blue OMI pixel and the average of the MODIS pixels (black). The grey curve indicates the OMI spectrum after scaling with the average MODIS spectrum.

3.5   Combining OMI-MODIS reflectances

After selection of suitable cloud pixels (step one), a hyperspectral reflectance spectrum was constructed using collocated OMI and MODIS/Aqua pixels. Spectrally, OMI overlaps with MODIS at 459–479 nm (central wavelength 469 nm), which can be used to match the OMI reflectances in the visible channel and the MODIS reflectance in band 3. Spatially, the overlap is more complicated, since the OMI footprint is not uniquely defined due to the use of a polarisation scrambler. The polarisation scrambler projects four depolarised beams onto the detector CCD, which are slightly shifted with respect to each other, and therefore only the central point of the OMI footprint is uniquely defined. Furthermore, since the optics of OMI contain no moving mirror, but projects the incoming radiation onto the CCD detector array directly during a 2-s interval, the spatial response function of the OMI footprints is not box-shaped, but rather Gaussian-shaped in two dimensions. 74% of the radiance received at a detector pixel is from within the corner coordinates, the rest of the signal is from outside the pixel corner coordinates. The OMI field of view was analysed in detail in de Graaf et al. (2016) and Sihler et al. (2017). A 2D-Gaussian shape is used here to average MODIS reflectances across the OMI pixel, favouring pixels near the OMI center and allowing for overlapping ground pixels.

The projections of radiation are slightly different in the two OMI UV channels and the OMI visible channel, resulting in slightly different ground pixels and wavelength grids, but these have not been accounted for. All computations were performed and reported relative to the wavelength grid and ground pixels of the OMI visible channel.

Two examples of OMI pixels tiled with MODIS pixels are shown in Figure 2. Figure 2a shows an overview of the situation; a broken cloud field over the south-east Atlantic Ocean, west of Africa, with two OMI pixels, one in the stratocumulus cloud deck (red), and one at the cloud edge (blue). Figure 2b shows the MODIS pixels that are collocated with the OMI pixels, colored by their weight in the averaging of the reflectance, which is the reflectivity convolved with the Gaussian function. Clearly, points close to the OMI pixel center are favored, but also pixels beyond the corner coordinates contribute to the radiation in the pixel. The cloud structure clearly has a large influence on the contributing pixels.

Figure 2c shows the combined OMI-MODIS reflectance of the fully cloudy scene (red), while Figure 2d shows the combined OMI-MODIS reflectance of the broken cloud scene (blue). Clearly, there is a mismatch between OMI and MODIS for the broken cloud scene, which is caused by rapid cloud changes. The average reflectance of the scene has changed during the 15 minutes between overpasses of Aura and Aqua. In order to get a contiguous reflectance spectrum, the average reflectance during the MODIS overpass is taken and OMI was scaled to match the MODIS average reflectance at 469 nm. Scaling MODIS to OMI seemed obvious at first, to have all parameters at the OMI grid and time. However, this resulted in very noisy data, because scaled MODIS reflectances resulted in flawed cloud parameter retrievals at longer wavelengths and the accuracy of the DRE over clouds depends strongly on the accuracy of the cloud parameters. The derivation of cloud parameters is treated below.

3.5.1   Cloud retrieval

In the current implementation, the MODIS reflectances at 1.2 μm and 2.1 μm are used to derive cloud droplet effective radius and cloud optical thickness, following Nakajima and King (1990) (step three). Using wavelengths in the SWIR, instead of

the visible, avoids biases of cloud parameters due to absorption by overlying aerosols (Haywood et al., 2004). The cloud parameters retrieved in this way have a larger uncertainty, but can be used for scenes with overlying aerosols (de Graaf et al., 2012). Note that the MODIS reflectance at 1.6 μm is not used for the cloud retrieval, because of the large number of bad and dead pixels in the MODIS/Aqua detector. The cloud droplet effective radius and cloud optical thickness are used to construct an aerosol-free cloud scene reflectance spectrum using RTM simulations ($R(\lambda)_{\mathrm{cld}}$ in Equation 3.) Since the retrieval of the DRE is depending so much on the correct cloud parameters and subsequent scene reflectance, the average MODIS reflectances
5 have to be taken as a basis, and OMI reflectances have to be scaled to MODIS. The cloud optical thickness and cloud effective radii are shown in Figure 2, representing the clouds in the two OMI pixels during MODIS overpass.

The combined, corrected reflectance spectra, as shown for the OMI pixels in Figure 2c and d, are the basis for the retrieval of the aerosol DRE over clouds using Equation 3.

4 Results

4.1 Aerosol DRE from combined OMI and MODIS reflectances

The aerosol DRE retrieval over clouds is illustrated using a case of smoke over the south-east Atlantic Ocean in August 2006. Retrieval results from both SCIAMACHY and combined OMI/MODIS measurements on 10 August 2006 are shown in Figure 3. August is the peak of the biomass burning season in southern Africa, and an extended smoke plume, originating from the African continent, is drifting over the ocean in an elevated layer above a stratocumulus deck in the boundary layer.

15 The presence of the smoke can be observed in the RGB images of Figures 3a and b as a gray haze over the continent, a darkening of the clouds and high DRE values due to absorption of radiation by smoke above the stratocumulus cloud deck. This cloud deck is typical for this part of the ocean due to upwelling at the east part of the basin, cooling the sea surface. The stratocumulus cloud deck is persistent in the south and breaks up towards the equator.

The vertical distribution of the aerosols and clouds is illustrated in Figure 3c, using CALIOP attenuated backscatter at
20 532 nm along a track shown in Figure 3a. It clearly shows the boundary layer stratocumulus clouds between 0–1 km altitude, rising towards the equator, and a thick smoke plume between 1–4 km altitude. The strong returns are the surface at 0 km and cirrus clouds around 12–14 km.

The smoke consists of small particles, which scatter and absorb the incoming sunlight. Scattering dominates and over a dark background like the ocean the planetary albedo is increased due to the smoke. This will result in a negative direct radiative
25 effect. However, over clouds the aerosol direct radiative effect becomes positive, because the cloud optical thickness is large and the aerosols do not contribute much to the scattering of the sunlight. They do however, absorb radiation in the visible and UV part of the shortwave spectrum, reducing the planetary albedo, resulting in a positive aerosol radiative effect over clouds. This is quantified by the OMI/MODIS aerosol DRE over clouds (Figure 3a).

The OMI/MODIS DRE reaches values up to 100 Wm^{-2} in parts where smoke from the African continent is abundant. The
30 values drop off to zero over clouds where the smoke plume is thinning and towards the cloud edges. The high and low values coincide well with concurrent measurements of SCIAMACHY DRE, shown in Figure 3b. This figure shows the SCIAMACHY
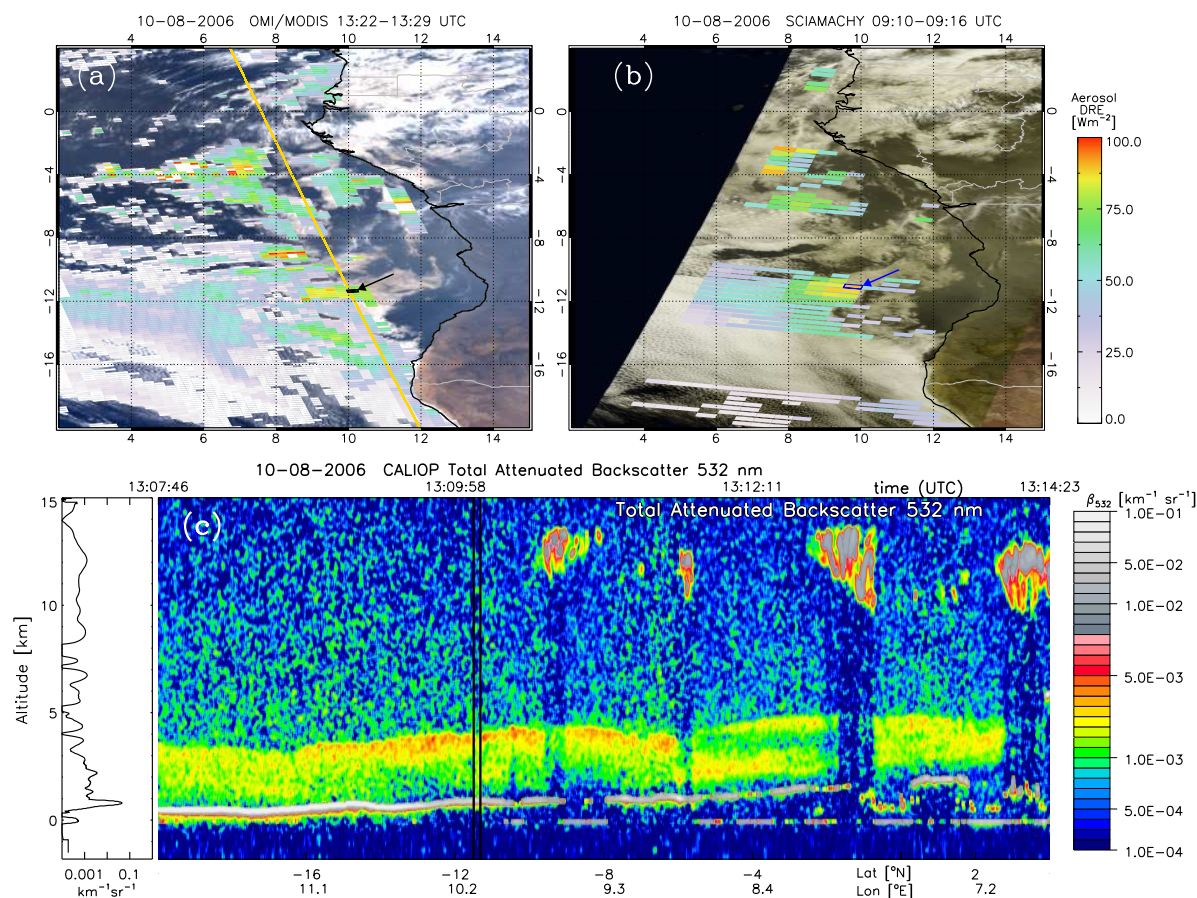
Figure 3. (a) Instantaneous Aerosol Direct Radiative Effect (DRE) over clouds on 10 August 2006 from a combination of OMI and MODIS reflectances, overlaid over a MODIS RGB image. The yellow line indicates the track of the backscatter profile by CALIOP that is shown in (c). The reflectance spectrum of the pixel indicated by the black arrow is given in Figure 4; (b) Aerosol DRE over clouds from SCIAMACHY, overlaid over a MERIS RGB image. The reflectance spectrum of the pixel indicated by the blue arrow is given in Figure 4; (c) CALIOP total attenuated backscatter at 532 nm in $km^{-1}sr^{-1}$ on 10 August 2006, for the yellow track indicated in (a). The location of the OMI pixel indicated in (a) by the arrow is indicated by the black vertical lines. The average CALIOP backscatter profile between the black lines is plotted on the left as a function of altitude.

DRE overlaid over a MERIS RGB image, both on Envisat. Obviously, the spatial coverage of SCIAMACHY is much lower than OMI and MODIS, measuring in nadir mode only half of the time, and having larger pixels. Consequently, the OMI/MODIS DRE is smoother with better coverage.

The location of the black OMI pixel (pointed at by the black arrow in Figure 3a,) coincides with the blue SCIAMACHY pixel in 3b (indicated by the blue arrow) and the black lines in Figure 3c. The computation of the DRE using the DAA thechnique for these pixels is illustrated in Figure 4. The OMI reflectance spectrum up to 500 nm of the black pixel is plotted in black,
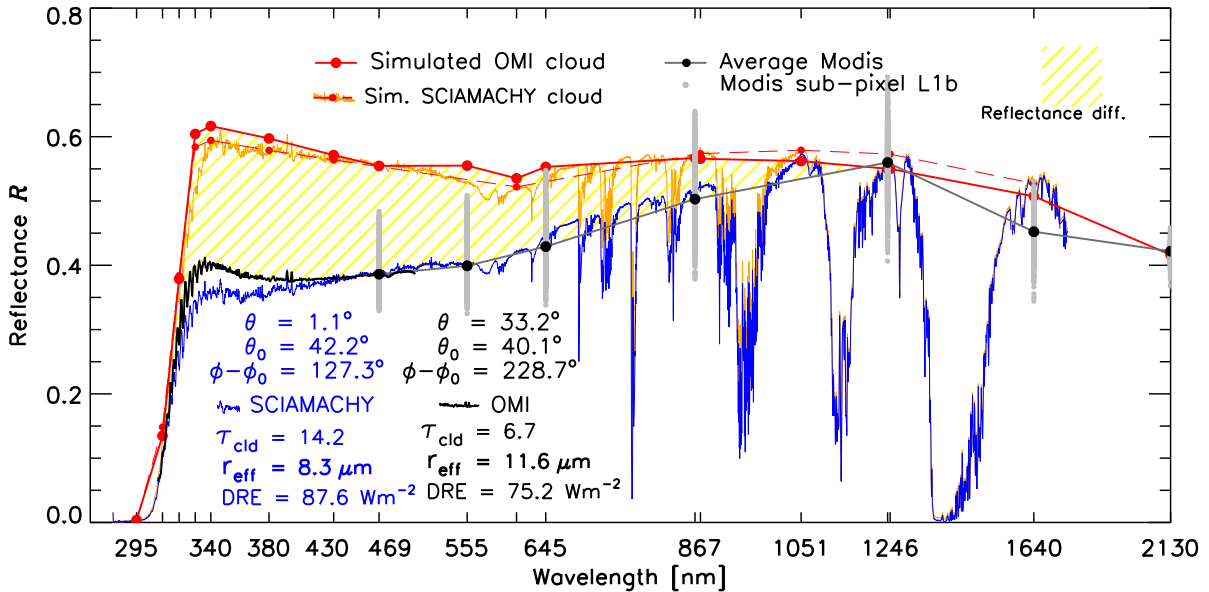
Figure 4. The differential Aerosol Absorption technique illustrated witj OMI/MODIS and SCIAMACHY spectra. In black the spectrum measured by OMI and MODIS is given for the pixel indicated by the black arrow in Figure 3a. In blue the SCIAMACHY measured spectrum is shown for the blue pixel in Figure 3b. The red solid line shows the simulated aerosol-free cloud spectrum computed with an RTM for the OMI pixel. The dashed red line shows the aerosol-free cloud spectrum simulated with an RTM for the SCIAMACHY pixel.

5   complemented with the average reflectance from collocated MODIS pixels (black dots). The variations in the reflectances of the individual MODIS pixels are shown by grey dots.

     The retrieved cloud droplet effective radius for this OMI scene was 11.6 μm, and the cloud optical thickness was 6.7. The aerosol-free cloud reflectance spectrum for this scene, computed with these cloud parameters (step four), is shown by the red solid line in Figure 4. By construction, the simulated reflectances match the MODIS measured reflectances at 1.2 μm and 2.1 μm. Note that the average MODIS reflectance at 1.6 μm does not match the simulated reflectance, due to dead and bad

5   pixels in this band.

     Comparing the black and red lines in Figure 4, differences can be observed between the simulated and measured reflectances by OMI and MODIS in the visible and UV. This is indicated by the yellow shaded area. The difference between the measured reflectance and the simulated scene reflectance is attributed to aerosol absorption by aerosols above the cloud layer in the real scene, which is not present in the simulated cloud-only scene, and used to compute the DRE following equation 3 (step five).

10   The DRE derived for this OMI scene was 75.2 Wm^{-2}.
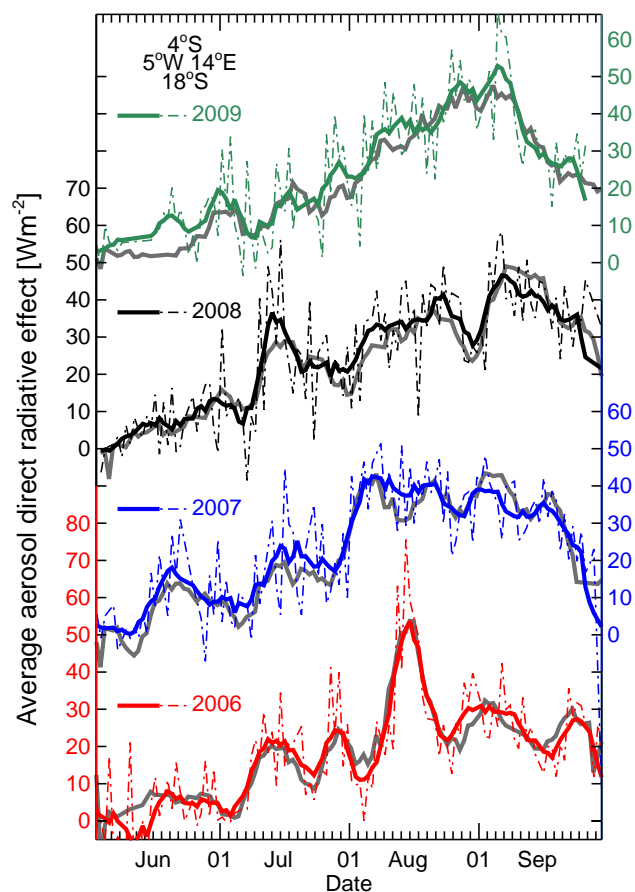
Figure 5. Daily area averaged aerosol DRE in Wm^{-2} for the region 4–18° S, 5° W–14°E (local overpass times from about 9:00–10:30 UTC) in 2006–2009 (thin lines) and its 7-day running mean (bold lines) in colored lines for all OMI/MODIS pixels with CF>0.3 and CP>800 hPa. In bold grey the SCIAMACHY area averaged aerosol DRE is plotted, which was published in de Graaf et al. (2014).

4.2 Comparison with SCIAMACHY

In the same Figure 4, the reflectance measured by SCIAMACHY is shown in blue, for the pixel indicated by the blue arrow in Figure 3b. This is a scene which is at the same location as the OMI pixel in Figure 3b, but measured three hours earlier. As can be seen in the RGB images, the cloud structures have changed rather considerably during this time, but the reflectance spectra from SCIAMACHY and OMI/MODIS are still remarkably similar. The DRE was also retrieved for this scene, using the SCIAMACHY reflectances at 1.2 μm and 1.6 μm. The cloud droplet effective radius during SCIAMACHY overpass was

5 8.3 μm and the cloud optical thickness was 14.2. The simulated aerosol-free cloud scene reflectance spectrum for these cloud parameters is shown in Figure 4 as the red dashed line. The SCIAMACHY DRE using the reflectance difference between the simulated cloud scene and the measured scene is 87.6 Wm^{-2}, which is slightly larger than observed by OMI. This is mainly due to the higher cloud optical thickness, for which the DRE is most sensitive.

The OMI/MODIS DRE is further compared with SCIAMACHY DRE over the south-east Atlantic area. SCIAMACHY has

10 been used before to analyse the impact of smoke during the African biomass burning season on the radiation budget (e.g. de Graaf et al., 2007, 2010). Very high daily and area averaged DRE were found in August 2006 of more than 80 Wm^{-2}, which could not be reproduced by global climate models (de Graaf et al., 2014). These high DRE values have since been confirmed by POLDER measurements (Peers et al., 2015), which show even higher instantaneous DRE values than those with SCIAMACHY. The daily, area-average DRE over the south-east Atlantic was also determined from OMI/MODIS com-

15 bined reflectances, and compared to the SCIAMACHY DRE (Figure 5). Only OMI pixels with an OMI O_2-O_2 cloud fraction (Veefkind et al., 2016) larger than 0.3 were selected, to ensure a sufficiently clouded scene, and only OMI pixels with an O_2-O_2 cloud pressure larger than 800 hPa, to exclude ice clouds. The SCIAMACHY data were similarly filtered, using FRESCO cloud fraction (Wang et al., 2012) larger than 0.3 and FRESCO cloud pressure larger than 800 hPa. The comparison is remarkably good, considering the much better OMI spatial coverage compared to that from SCIAMACHY. Pearson's correlation coeffi-

20 cient for the seven-day averaged DRE values from SCIAMACHY and OMI/MODIS is 0.9667. A fit between the two datasets showed that the DRE from OMI/MODIS was about 5% lower than that retrieved from SCIAMACHY on average with an offset of 2.4 Wm^{-2}. The average aerosol DRE over clouds in August 2006 was 31.5 Wm^{-2} with a standard deviation of 16 Wm^{-2} from OMI/MODIS measurements, while it was 32.4 Wm^{-2} with a standard deviation of 17 Wm^{-2} from SCIAMACHY mea- surements. The maximum daily averaged DRE from OMI/MODIS in August 2006 was 75.6 $\pm$ 13 Wm^{-2}, from SCIAMACHY

25 it was 86.7 $\pm$ 8 Wm^{-2}.

A comparison between these datasets and an independent dataset retrieved from POLDER data confirms the close correlation even for individual pixels if the datasets are corrected for all sampling issues as best as possible (de Graaf et al., 2019). This shows once again the large impact of African smoke on the local radiation budget over the south-east Atlantic.

4.3 Accuracy assessment

30 In order to provide an error estimate for the OMI/MODIS DRE measurements, the uncertainty ϵ in equation 3 is analysed in this section. The most important error source is the modeling of unpolluted cloud spectra, or the ability to represent an aerosol-free
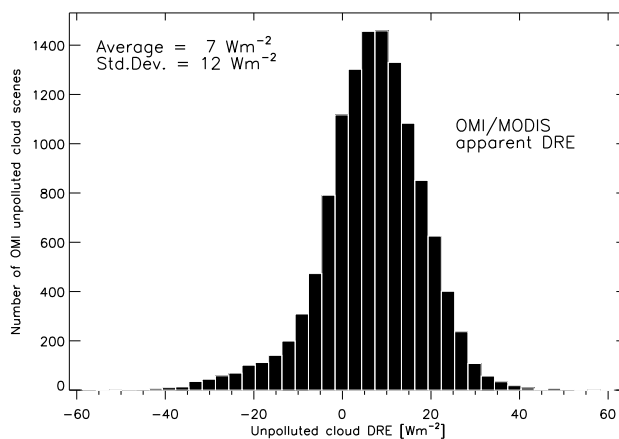
Figure 6. Frequency distribution of the apparent aerosol effect of all OMI aerosol-unpolluted marine water cloud scenes in June–Sept. 2006 over the South Atlantic Ocean (20° S–10° N, 10° W–20° E). The OMI/MODIS DRE for each pixel with OMI AAI < 0, CF > 0.3 and CP > 800 hPa was considered. The offset (apparent DRE) for these pixels is 7 Wm^{-2}, which is taken as the bias of the OMI/MODIS DRE method. The standard deviation of the DRE for these unpolluted scenes is 12 Wm^{-2}, which is a measure of the random error of the DRE.

cloud spectrum by a simulated spectrum. This assumption can readily be tested by comparing measured aerosol-free cloud spectra $R_{\mathrm{cld}}^{\mathrm{meas}}$ to simulated spectra $R_{\mathrm{cld}}^{\mathrm{sim}}$ for scenes that are screened for absorbing aerosols, as explained in section 2.2. The difference $R_{\mathrm{cld}}^{\mathrm{meas}} - R_{\mathrm{cld}}^{\mathrm{sim}}$ should ideally be zero, so the resulting aerosol DRE from these scenes should be zero. Figure 6 shows the aerosol DRE for all scenes in June–August 2006 with an UV-AI smaller than 0, to ensure the absence of absorbing aerosols (de Graaf et al., 2005), an OMI O$_2$-O$_2$ cloud fraction larger than 0.3 to ensure a sufficiently clouded scene, and an OMI O$_2$-O$_2$ cloud pressure higher than 800 hPa, to exclude ice clouds. The average difference in DRE between the simulated and

5   real scenes was about 7 Wm^{-2}, which represents a systematic error of the differential absorption technique for OMI/MODIS scenes. This error was determined for each year separately and corrected for so the average DRE for aerosol-free cloud scenes is zero. The standard deviation for the apparent DRE between simulated and real spectra was 12 Wm^{-2}, which is a random error in this term.

Other error sources were treated in de Graaf et al. (2012), like the unchanged anisotropy factor B between polluted and

10   unpolluted scenes, the effect of aerosol absorption on cloud fraction and cloud pressure retrievals, and the assumption of zero aerosol absorption at 1.2 microns. All these errors were found to be small, in the order of about 1 Wm^{-2}. Here, we assume that the random errors from these errors sources are similar to those for SCIAMACHY and independent, so they can be added using standard error propagation theory. This way, the error in OMI/MODIS DRE retrievals is found to be about 13 Wm^{-2}, which was almost twice that for SCIAMACHY DRE. The mean reason for this decrease in accuracy is the combination of

15   measurements from OMI and MODIS, which do not observe a scene at exactly the same time.
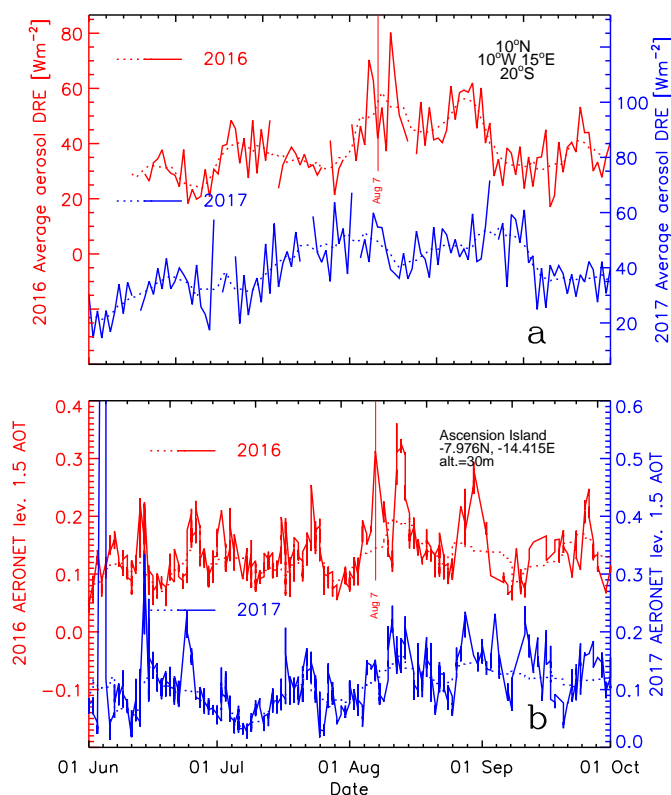
Figure 7. Top panel: OMI/MODIS Aerosol DRE over clouds, averaged over the Atlantic Ocean (10° N–20° S; 10° W–15° E) in 2016 (red) and 2017 (blue). The solid line shows the daily average, the dashed line shows a 7-day running mean. Bottom panel: AERONET AOT at 500 nm from Ascension Island station at 7.98° S, 14.42° W in 2016 (red) and 2017 (blue). The solid line shows all available level 1.5 data, the dashed line shows a 100 point running mean.

5   CLARIFY-ORACLES-LASIC campaigns

During 2016 and 2017, several field campaigns have been performed in the south-east Atlantic region. From May 2016 until October 2017, an ARM Mobile Facility was installed and run on Ascension Island, providing ground-based remote sensing and *in situ* measurements of clouds and aerosols (Zuidema et al., 2018). Also in 2016 and 2017, aircraft measurement campaigns have been carried out from Namibia, Ascension Island and São Tomé, to sample clouds and aerosols microphysical parameters, and measure radiation (Zuidema et al., 2016).

5   In support of these campaigns, the aerosol DRE over clouds averaged over the south-east Atlantic was computed using combined OMI/MODIS reflectances from 1 June–1 October in 2016 and 2017 for pixels with a cloud fraction larger than 0.3 and cloud pressure larger than 800 hPa, see Figure 7a. Daily averages are shown by the solid line, the dashed line shows a seven day running mean. It shows the evolution of smoke from vegetation fires in Africa over the ocean. In 2016, the amount of
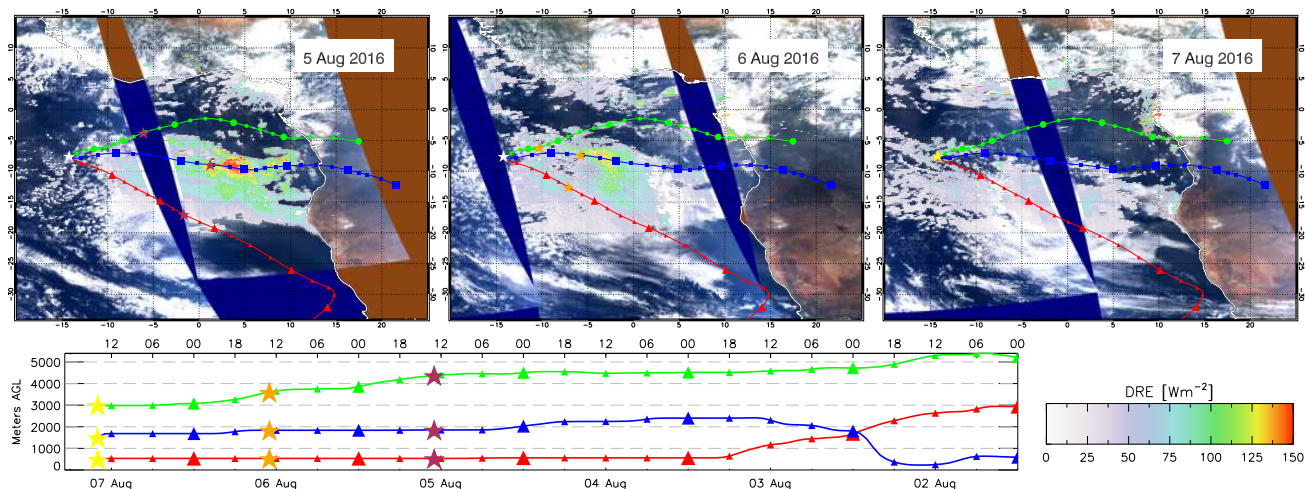
Figure 8. Aerosol DRE over clouds from OMI/MODIS overlaid over MODIS RGB images for three consecutive days (5–7 August), and backtrajectories from Ascension Island of air parcels ending at 500 m (red), 1500 m (blue) and 3000 m (green). The position of the air in the backtrajectories during the satellite overpasses is indicated by the coloured stars (yellow on 7 Aug. (at Ascension Island), orange on 6 Aug. and brown on 5 Aug.)

smoke is moderate in all months, except in August, when two periods of extreme pollution over the ocean can be observed. In 2017, a gradual increase of the pollution amount is observed from June onward, until it quickly diminishes halfway September. These differences can be caused by meteorological differences, controlling the transport of the smoke from the continent to the ocean, and by differences in the amount of fires, which is in turn also determined by meteorological factors (droughts and the onset of the rain season).

The high values of the aerosol DRE in August and September 2016 are reflected in AOT data collected by the AERONET station on Ascension Island, located at 8°S, 14.4°W. The AOT at 500 nm over Ascension Island from 1 June–1 October 2016 and 2017 is shown in Figure 7b. It shows AOT higher than 0.2 in a few isolated events in August 2016, which were strongly correlated with episodes of high aerosol DRE over clouds in the South Atlantic, as shown in Figure 7a. On the other hand, in 2017 the aerosol DRE values were more moderate, and do not correlate clearly with the AOT over Ascension Island.

The peaks in AOT over Ascension Island lag the peaks in DRE over the Atlantic by two days. This is shown for 7 August 2016 (vertical line in Figure 7) and Figure 8, which presents the aerosol DRE from OMI/MODIS during three days: 5, 6, and 7 August 2016. On the first day the aerosol DRE over the Atlantic Ocean peaks (Figure 7a), while during the last day the AOT over Ascension peaks (Figure 7b).

In Figure 8, HYSPLIT backtrajectories (Rolph et al., 2017) of air parcels ending over Ascension Island at 500, 1500, and 3000 m altitude are overlaid over each image (same trajectories in all images). They show the rapid transport of smoke over the Atlantic originating from Angola and its back-country. The colored stars indicate the time of satellite overpass in each

backtrajectory, which is around 13 UTC. On August 5 this is indicated by the brown stars, on August 6 by orange stars, while on August 7 this is at Ascension, indicated by the yellow star.

The wind direction in the boundary layer (500 m, red) is south-east, which is very persistent for this area. The air ending at 1500 m (blue) originates from Angola and beyond, while the air at 3000 m (green) originated somewhere around Congo. All three layers can carry aerosols and contribute to the high AOT at Ascension Island.

The boundary layer will likely contain marine aerosols, but the transport in this layer is very constant, adding to the back-
5 ground AOT over Ascension of about $0.1 - 0.2$. Only the 1500 m layer coincides exactly with the peak DRE over the ocean during 5 and 6 August, as shown by the stars in the different panels. High values of DRE travel along the blue 1500 m line, crossing the Atlantic in only a few days. Interestingly, the altitude of this layer (shown in the bottom layer of Figure 8) is close to the ground over the continent, quickly rising to above 2000 m at some point and then gradually declining to 1500 m. This strongly suggests that the layer is smoke filled and heated over a fire area, which then travels over the ocean in a stable elevated
10 layer, as found by Swap et al. (1996). Lastly, the layer ending at 3000 m is at a high altitude at all times, and is not collocated with high DRE values, and therefore it is less likely that this layer contributes to the high AOT over Ascension.

6 Conclusions

In this paper, the aerosol direct radiative effect product is presented retrieved from combined level 1B reflectance measurements from OMI and MODIS. The synergistic use of multiple instruments was made possible because the instruments fly in formation
15 in the A-train. This presents opportunities which are not otherwise possible, or with a much lower coverage, depending on the collocation of instruments.

The aerosol DRE over clouds can be retrieved from combined OMI/MODIS reflectance spectra using the DAA technique, as it was also done using SCIAMACHY spectra. MODIS reflectance collocated with OMI pixels were used to retrieve cloud properties of a cloud scene, while the combined OMI and MODIS shortwave reflectance spectrum provides information about
20 the absorption by aerosols in the UV and visible part of the spectrum.

This yields aerosol DRE over clouds which were compared with existing data from SCIAMACHY, using cloud scenes over the Atlantic Ocean. This area is known for its strong pollution by smoke during the south African biomass burning season, and can be used to demonstrate the strong aerosol DRE over clouds. The average aerosol DRE over clouds in August 2006 was 31.5 Wm^{-2} with a standard deviation of 16 Wm^{-2}. The maximum daily averaged DRE from OMI/MODIS in August 2006
25 was $75.6 \pm 13 \text{ Wm}^{-2}$. The OMI/MODIS DRE shows a very good correlation with SCIAMACHY DRE between 2006–2009, and has a much better resolution and coverage. Furthermore, SCIAMACHY stopped delivering data in 2012, while OMI and MODIS are still producing high quality data.

OMI/MODIS DRE data in 2016 and 2017 show the effect of smoke being transported over the Atlantic all the way to Ascension, 3000 km from its source, where it coincides with high AOT values measured by AERONET. Backtrajectories
30 show the altitude of the smoke layer above the boundary layer in the free troposphere, as found by several studies before. The

OMI/MODIS DRE can be used to study the aerosol direct effect, but also contribute to understanding more complex feedback mechanisms between clouds, aerosols and radiation.

Data availability. The OMI/MODIS DRE is freely available from the first author on request.

Author contributions. MdG developed the DAA technique, its application to OMI/MODIS measurements and created the SCIAMACHY and OMI/MODIS DRE datasets. LGT provided support for the satellite retrievals and developed surface reflectance datasets. PS developed the RTM

5 *Competing interests.* NA

Acknowledgements. This work was funded by the Dutch National Programme for Space Research User of the Netherlands Space Office (NSO), projectnumber ALW-GO/12-32. Brent Holben is thanked as PI of the AERONET station at Ascension Island and providing the AOT data.

References

10   Alfaro-Contreras, R., Zhang, J., Campbell, J. R., Holz, R. E., and Reid, J. S.: Evaluating the impact of aerosol particles above cloud on cloud optical depth retrievals from MODIS, Journal of Geophysical Research: Atmospheres, 119, 5410–5423, https://doi.org/10.1002/2013JD021270, 2014.

Bhartia, P. K., McPeters, R. D., Flynn, L. E., Taylor, S., Kramarova, N. A., Frith, S., Fisher, B., and DeLand, M.: Solar Backscatter UV (SBUV) total ozone and profile algorithm, Atmos. Meas. Tech., 6, 2533–2548, https://doi.org/10.5194/amt-6-2533-2013, 2013.

5   Bovensmann, H., Burrows, J. P., Buchwitz, M., Frerick, J., Noël, S., Rozanov, V. V., Chance, K. V., and Goede, A. P. H.: SCIAMACHY: Mission Objectives and Measurement Modes, J. Atmos. Sci., 56, 127–150, https://doi.org/10.1175/1520-0469, 1999.

Burrows, J. P., Weber, M., Buchwitz, M., Rozanov, V., Ladstätter-Weißenmayer, A., Richter, A., DeBeek, R., Hoogen, R., Bramstedt, K., Eichmann, K. -U., Eisinger, M., and Perner, D.: The Global Ozone Monitoring Experiment (GOME): Mission Concept and First Scientific Results, J. Atmos. Sci., 56, 151–175, https://doi.org/10.1175/1520-0469, 1999.

10   de Graaf, M., Stammes, P., Torres, O., and Koelemeijer, R. B. A.: Absorbing Aerosol Index: Sensitivity Analysis, application to GOME and comparison with TOMS, J. Geophys. Res., 110, D01201, https://doi.org/10.1029/2004JD005178, 2005.

de Graaf, M., Stammes, P., and Aben, E. A. A.: Analysis of reflectance spectra of UV-absorbing aerosol scenes measured by SCIAMACHY, J. Geophys. Res., 112, D02206, https://doi.org/10.1029/2006JD007249, 2007.

de Graaf, M., Tilstra, L. G., Aben, I., and Stammes, P.: Satellite observations of the seasonal cycles of absorbing aerosols in Africa related to
15   the monsoon rainfall, 1995 - 2008., Atmos. Environ., 44, 1274–1283, https://doi.org/10.1016/j.atmosenv.2009.12.03, 2010.

de Graaf, M., Tilstra, L. G., Wang, P., and Stammes, P.: Retrieval of the aerosol direct radiative effect over clouds from spaceborne spectrom-etry, J. Geophys. Res., 117, https://doi.org/10.1029/2011JD017160, http://dx.doi.org/10.1029/2011JD017160, 2012.

de Graaf, M., Bellouin, N., Tilstra, L. G., Haywood, J., and Stammes, P.: Aerosol direct radiative effect of smoke over clouds over the southeast Atlantic Ocean from 2006 to 2009, Geophys. Res. Lett., https://doi.org/10.1002/2014GL061103,
20   http://dx.doi.org/10.1002/2014GL061103, 2014.

de Graaf, M., Sihler, H., Tilstra, L. G., and Stammes, P.: How big is an OMI pixel?, Atmos. Meas. Tech., https://doi.org/10.5194/amt-9-3607-2016, http://www.atmos-meas-tech.net/9/3607/2016/, 2016.

de Graaf, M., Schulte, R., Peers, F., Waquet, F., and Stammes, P.: Comparison of Aerosol Direct Effect over clouds, Geophys. Res. Lett., *in prep.*, xx – xx, 2019.

25   Fleig, A. J., Bhartia, P. K., Wellemeyer, C. G., and Silberstein, D. S.: Seven years of total ozone from the TOMS instrument-A report on data quality, Geophys. Res. Lett., 13, 1355–1358, https://doi.org/10.1029/GL013i012p01355, 1986.

Forster, P., Ramaswamy, V., Artaxo, P., Berntsen, T., Betts, R., Fahey, D. W., Haywood, J., Lean, J., Lowe, D. C., Myhre, G., Nganga, J., Prinn, R., Raga, G., Schulz, M., and Van Dorland, R.: Contribution of Working Group I to the Fourth Assessment Report of the Intergovernmental Panel on Climate Change, in: Climate Change 2007: The Physical Science Basis., edited by Solomon, S., Qin, D., Manning, M., Chen, Z.,
30   Marquis, M., Averyt, K., Tignor, M., and Miller, H., p. 996, Cambridge Univ. Press, Cambridge, UK and New York, NY, USA, 2007.

Haywood, J. and Boucher, O.: Estimates of the direct and indirect radiative forcing due to tropospheric aerosols: A review, Rev. Geophys., 38, 513–543, 1999RG000078, 2000.

Haywood, J. M., Osborne, S. R., and Abel, S. J.: The effect of overlying absorbing aerosol layers on remote sensing retrievals of cloud effective radius and cloud optical depth, Q. J. R. Meteorol. Soc., 130, 779–800, https://doi.org/10.1256/qj.03.100, 2004.

35 Levelt, P. F., van den Oord, G. H. J., Dobber, M. R., Mälkki, A., Visser, H., de Vries, J., Stammes, P., Lundell, J. O. V., and Saari, H.: The ozone monitoring instrument, IEEE T. Geosci. Remote, 44, 1093–1101, 2006.

Lohmann, U. and Feichter, J.: Global indirect aerosol effects: a review, Atmos. Chem. Phys., 5, 2005.

Nakajima, T. and King, M. D.: Determination of the Optical Thickness and Effective Particle Radius of Clouds from Reflected Solar Radiation Measurements: Part I: Theory, J. Atmos. Sci., 47, 1990.

Peers, F., Waquet, F., Cornet, C., Dubuisson, P., Ducos, F., Goloub, P., Szczap, F., Tanré, D., and Thieuleux, F.: Absorption of aerosols above
5   clouds from POLDER/PARASOL measurements and estimation of their direct radiative effects, Atmos. Chem. Phys., 15, 4179–4196, https://doi.org/10.5194/acp-15-4179-2015, 2015.

Rolph, G., Stein, A., and Stunder, B.: Real-time Environmental Applications and Display sYstem: READY, Environ. Modell. Softw., 95, 210 – 228, https://doi.org/10.1016/j.envsoft.2017.06.025, 2017.

Sihler, H., Lübcke, P., Lang, R., Beirle, S., de Graaf, M., Hörmann, C., Lampel, J., Penning de Vries, M., Remmers, J., Trol-
10 lope, E., Wang, Y., and Wagner, T.: In-operation field-of-view retrieval (IFR) for satellite and ground-based DOAS-type instruments applying coincident high-resolution imager data, Atmos. Meas. Tech., 10, 881–903, https://doi.org/10.5194/amt-10-881-2017, https://www.atmos-meas-tech.net/10/881/2017/, 2017.

Swap, R., Garstang, M., Macko, S. A., Tyson, P. D., Maenhaut, W., Artaxo, P., Kållberg, P., and Talbot, R.: The long-range transport of southern African aerosols to the tropical South Atlantic, J. Geophys. Res., 101, D19, https://doi.org/10.1029/95JD01049, 1996.

15 Veefkind, J. P., de Haan, J. F., Sneep, M., and Levelt, P. F.: Improvements to the OMI O_2–O_2 operational cloud algorithm and comparisons with ground-based radar–lidar observations, Atmos. Meas. Tech., 9, 6035–6049, https://doi.org/10.5194/amt-9-6035-2016, https://www.atmos-meas-tech.net/9/6035/2016/, 2016.

Wang, P., Tuinder, O. N. E., Tilstra, L. G., de Graaf, M., and Stammes, P.: Interpretation of FRESCO cloud retrievals in case of absorbing aerosol events, Atmos. Chem. Phys., 12, 9057–9077, https://doi.org/10.5194/acp-12-9057-2012, 2012.

20 Wilcox, E. M.: Direct and semi-direct radiative forcing of smoke aerosols over clouds, Atmos. Chem. Phys., 12, 139–149, https://doi.org/10.5194/acp-12-139-2012, 2012.

Yu, H. and Zhang, Z.: New Directions: Emerging satellite observations of above-cloud aerosols and direct radiative forcing, Atmos. Environ., 72, 36–40, https://doi.org/http://dx.doi.org/10.1016/j.atmosenv.2013.02.017, 2013.

Yu, H., Kaufman, Y. J., Chin, M., Feingold, G., Remer, L. A., Anderson, T. L., Balkanski, Y., Bellouin, N., Boucher, O., Christopher, S.,
25 DeCola, P., Kahn, R., Koch, D., Loeb, N., Reddy, M. S., Schulz, M., Takemura, T., and Zhou, M.: A review of measurement-based assessments of the aerosol direct radiative effect and forcing, Atmos. Chem. Phys., 6, 613–666, https://doi.org/10.5194/acp-6-613-2006, http://www.atmos-chem-phys.net/6/613/2006/, 2006.

Zuidema, P., Redemann, J., Haywood, J., Wood, R., Piketh, S., Hipondoka, M., and Formenti, P.: Smoke and Clouds above the South-east Atlantic: Upcoming Field Campaigns Probe Absorbing Aerosol's Impact on Climate, Bull. Am. Meteor. Soc., 97, 1131–1135,
30 https://doi.org/10.1175/BAMS-D-15-00082.1, 2016.

Zuidema, P., Sedlacek III, A. J., Flynn, C., Springston, S., Delgadillo, R., Zhang, J., Aiken, A. C., Koontz, A., and Muradyan, P.: The Ascension Island Boundary Layer in the Remote Southeast Atlantic is Often Smoky, Geophys. Res. Lett., 45, 4456–4465, https://doi.org/10.1002/2017GL076926, https://agupubs.onlinelibrary.wiley.com/doi/abs/10.1002/2017GL076926, 2018.